JOURNAL OF MATERIALS SCIENCE 35 (2000) 4093–4098

Hydrogen reduction of a RuO_2 electrode prepared by DC reactive sputtering

Y. MATSUI, M. HIRATANI, S. KIMURA
Central Research Laboratory, Hitachi, Ltd., Tokyo, 185-8601, Japan
E-mail: y-Matsui@crl.hitachi.co.jp

RuO_2 thin films deposited by reactive DC sputtering were heat-treated in a 0.3%-H_2 atmosphere at 200°C in order to investigate the reduction property of RuO_2. The films were selectively reduced (starting from the interface) because of insufficient oxidation. When the as-deposited RuO_2/Si structure was hydrogen-reduced, the RuO_2 film was broken into fragments because of poor mechanical strength. On the other hand, the RuO_2 film heat-treated once in O_2 at 700°C cracked into a star shape as a result of vapor generation and volume shrinkage. The star-shape cracking was still observed even when the RuO_2 film was covered with a 90-nm-thick BST film. The mechanical strength and the adhesion of RuO_2 were improved to some extent by post-oxidation at high temperatures. However, a way to prevent the morphological destruction could not be found because of the thermodynamic equilibrium during the hydrogen reduction process.

1. Introduction

Ruthenium dioxide (RuO_2) exhibits various interesting characteristics such as metallic conductivity, excellent diffusion barrier nature [1–6] and dry etching property capable of fine patterning [7, 8]. In addition, (Ba, Sr)TiO_3 [BST] can be deposited on RuO_2 film at high temperatures over 500°C, so a stable electrode/dielectrics interface is formed. Therefore, RuO_2 film is a promising bottom electrode of oxide dielectrics capacitors in Gbit-scale dynamic random access memories (DRAMs) [9–11].

However, it has been reported that RuO_2 is reduced to Ru metal after heat-treatment in a vacuum at temperatures above 450°C [11]. This suggests that RuO_2 is chemically unstable under a reducing atmosphere. On the other hand, during fabrication, DRAMs must be treated in a dilute hydrogen gas after capacitor integration in order to reduce the density of the traps at the SiO_2/Si interface of metal-oxide-semiconductor field-effect transistors (MOSFETs). If the RuO_2 electrode cannot stand the reducing process, the capacitance will be degraded and the capacitor itself will be damaged by the volume change. The hydrogen reduction must be fully understood in order to apply the RuO_2 film to the bottom electrode and the integration process in DRAMs.

In this study, the RuO_2 thin film was deposited by a reactive DC sputtering and was treated in a 0.3%-H_2 atmosphere at 200°C. And the destruction process of the RuO_2 electrode during hydrogen reduction was examined in detail.

2. Experiments

RuO_2 thin films were deposited on Si substrates and Ru (50-nm thick)/TiN (80-nm thick)/Ti (50-nm thick)/Si structures by reactive DC sputtering using a Ru metal target. TiN is a diffusion barrier and Ti is an adhesive layer between TiN and Si, both of which are often used in capacitor electrodes [9]. For deposition on the Si substrate, total pressure was 0.10 Pa, Ar/O_2 discharge gas ratio was 2 sccm/30 sccm (oxygen partial pressure P_{O2}, of 0.09 Pa) and incident power was 2 kW. And for deposition on the Ru/TiN/Ti/Si structure, total pressure was 0.53 Pa, Ar/O_2 gas ratio was 10 sccm/90 sccm (P_{O2} of 0.48 Pa), and incident power was 1 kW. Deposition temperature was 300°C and film thickness was 200 nm under both conditions. To assure crystallization, some samples were heat-treated in O_2 for 15 min at temperatures ranging from 500°C to 700°C.

BST thin films were deposited on the RuO_2/Si structure by pulsed laser deposition (PLD); deposition temperature was 500°C, oxygen pressure was 13.3 Pa, and film thickness was 90 nm. These three structures, RuO_2/Si, BST/RuO_2/Si, and RuO_2/Ru/TiN/Ti/Si, were reduced in a mixed 0.3%-H_2/Ar gas flow at 200°C for 15 min.

The crystallographic properties were evaluated by using low-angle incident x-ray diffraction with a fixed incident angle of 2°. The Cu K_α line was used as an x-ray source, incident power was 40 kV at 150 mA, and scanning rate was 2°/min. The surface and cross-sectional morphologies of the films were observed by optical microscope and scanning electron microscope (SEM).

3. Results and discussion

3.1. Hydrogen reduction of RuO_2 film on a Si substrate

Fig. 1 shows x-ray diffraction patterns of 200-nm-thick RuO_2 thin films on the Si substrate. Lines (a) and (b)

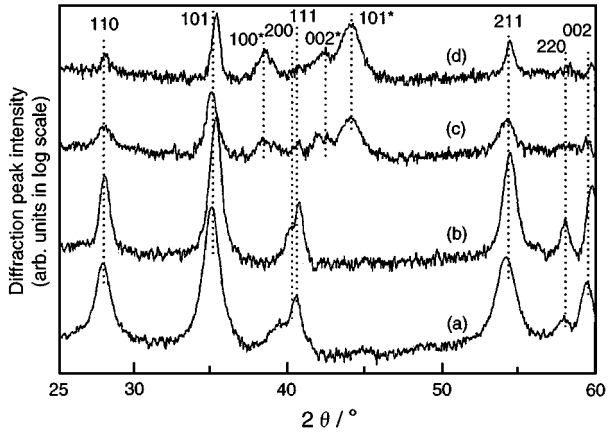

Figure 1 x-ray diffraction patterns of RuO_2 on Si: (a) as-deposited, (b) after O_2-heat treatment at 700°C, (c) after 0.3%-H_2 reduction at 200°C, (d) after 0.3%-H_2 reduction at 200°C via O_2-heat treatment at 700°C. Indices *hkl* and *hkl** indicate RuO_2 and Ru, respectively.

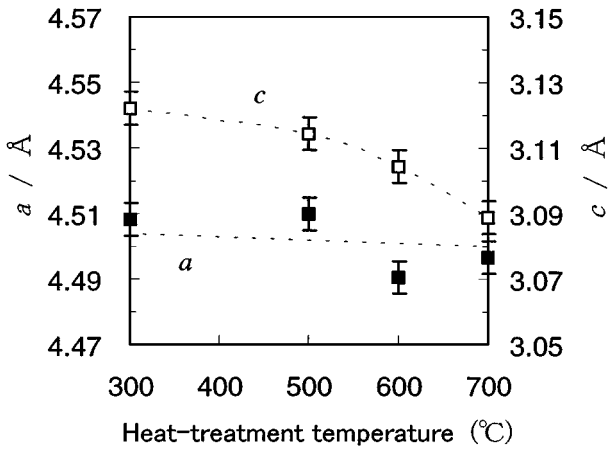

Figure 2 Variation of lattice constants with heat-treatment in O_2.

represent the as-deposited RuO_2 film and the one heat-treated at 700°C in O_2 after the deposition. Lines (c) and (d) represent the patterns after 0.3%-H_2 reduction at 200°C of the films represented by (a) and (b), respectively. Indices *hkl* indicate the diffraction peaks from RuO_2, and indices *hkl** are assignable to the Ru metal. The O_2 heat treatment hardly affected the diffraction pattern except for a slight peak shift. Fig. 2 indicates the dependence of the lattice constant on the O_2-heat-treatment temperature. With increasing heat treatment temperature, the *a*-axis length is almost constant but the *c*-axis remarkably decreases. This *c*-axis shrinkage does not depend on the heat treatment atmosphere (either Ar or O_2). In addition, the lattice constants do not change after the hydrogen reduction at 200°C (not shown in the figure). Consequently, it can be concluded that oxygen vacancies are not responsible for the *c*-axis shrinkage. It is reasonable to think that the thermal contribution from the heat treatment, which is higher than the RuO_2 deposition temperature (300°C), mainly dominates the lattice shrinkage. Actually, the lattice constant approached the bulk value (*a*-axis: 4.50 Å, *c*-axis: 3.11 Å [12]); that is, the RuO_2 film is better-crystallized by heat treatment at 700°C. On the other hand, the hydrogen reduction decreased the diffraction peak intensity of RuO_2 to approximately a tenth of the original intensity, at the same time, Ru metal was formed as a reducing product [Lines (c) and (d) in Fig. 1]. In brief, Fig. 1 demonstrates that RuO_2 was partially reduced to Ru metal regardless of whether it was well-crystallized.

However, the effect of heat treatment at 700°C on the crystallization is dramatic when we compare the surface morphology of the film before and after hydrogen reduction, as shown in Fig. 3. The RuO_2 film was broken into fragments (Fig. 3a), when the RuO_2/Si structure was hydrogen-reduced without O_2-heat treatment. On the other hand, the RuO_2 film once heat-treated in O_2 at 700°C cracked into a distinguished morphology (Fig. 3b). In region A, the RuO_X film (dark gray) cracks into a star shape (light gray), and the Si substrate (medium gray) of the underlayer is showing through the inside of the star-shape cracks. In region B where most of RuO_X film peeled off and the Si substrate is recognized as the medium-gray surface, the residual RuO_X films appear as the enclosed dark-gray region, so the star-shape cracks appear similar to those in region A.

The mechanism of the star-shape cracking by hydrogen reduction can be explained as follows. Fig. 4 shows star-shape cracks with several sizes ranging from a few microns to tens of microns. All the stars inscribe a real circle. Fig. 5 shows the detail of a star-shape crack. The circle drawn inside the crack is concentric with the outer circle that the star-shape crack inscribes. In the enlarged photograph of Fig. 5b, a facing edge of the crack was duplicated mechanically and put along the opposite edge. The irregular crack front fits the opposite edge well, demonstrating that edges moved off after the crack formation as indicated by the white arrows.

The precise process of the cracking is described in Fig. 6. First, the hydrogen gases diffuse through the RuO_2 film, and reach the RuO_2/Si interface (Fig. 6a). Here, the Si substrate surface was preferentially oxidized during the RuO_2 film preparation because of the difference of the Gibbs' formation free energy between SiO_2 and RuO_2 $\{\Delta G^0(SiO_2) = -684\ \text{kJ mol}^{-1} < \Delta G^0(RuO_2) = -213\ \text{kJ mol}^{-1}$ at 300°C [13]$\}$. Then, it is thought that the RuO_2 at the interface is not sufficiently oxidized and is less tolerant to hydrogen reduction. The reduction of RuO_2, together with generation of water vapor, starts at the interface according to the following reaction:

$$RuO_2 + 2H_2 \Leftrightarrow Ru + 2H_2O \qquad (1)$$

The RuO_2 film keeps the vapor pressure uniform, and then the film is peeled off at the RuO_2/Si interface and forms a dome as shown in Fig. 6b. Further RuO_2 reduction across the film toward the surface causes the star-shape crack to form from the dome's apex (Fig. 6c). This is because the film volume shrinks to a half accompanied by the reduction from RuO_2 to Ru. Namely, both effects of vapor generation and volume shrinkage cause the star-shape cracks which inscribe a circle. However, without post-heat treatment at 700°C, the film breaks into irregular pieces at random (Fig. 3a), since the film cannot hold the vapor pressure because of the poor mechanical strength.

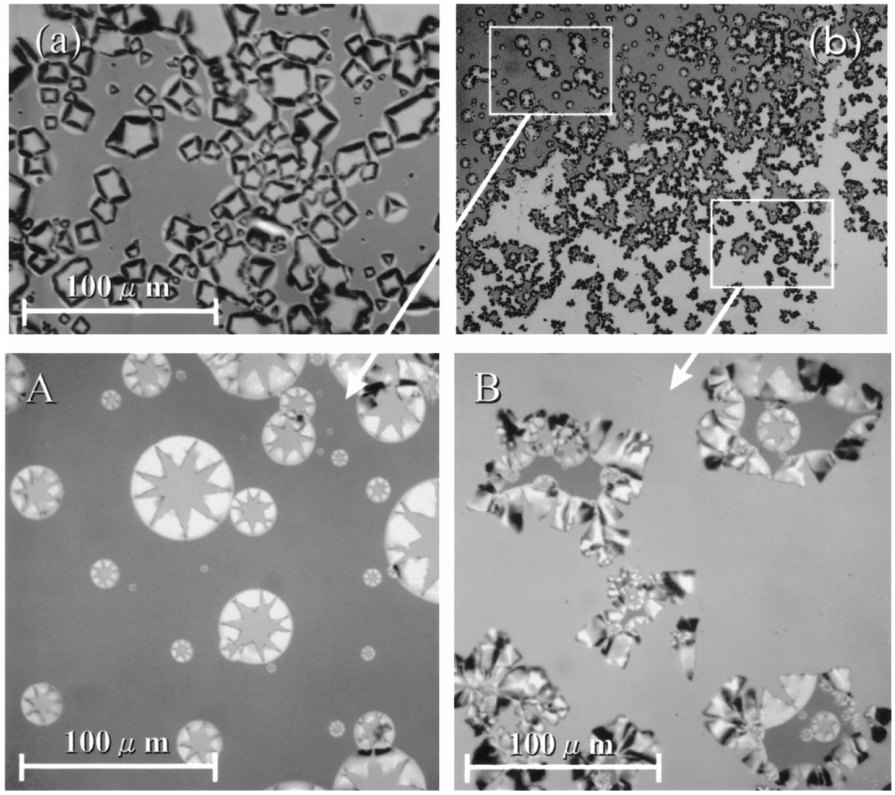

Figure 3 Optical microscope photographs of RuO_X/Si: (a) after 0.3%-H_2 reduction at 200°C (the same film as in Fig. 1c), and (b) after 0.3%-H_2 reduction at 200°C via O_2-heat treatment at 700°C (the same film as in Fig. 1d). The star-shape cracks are conspicuous. The dark gray region is RuO_2, the medium gray region is Si substrate showing through the cracks, and the light-gray region is reduced RuO_2.

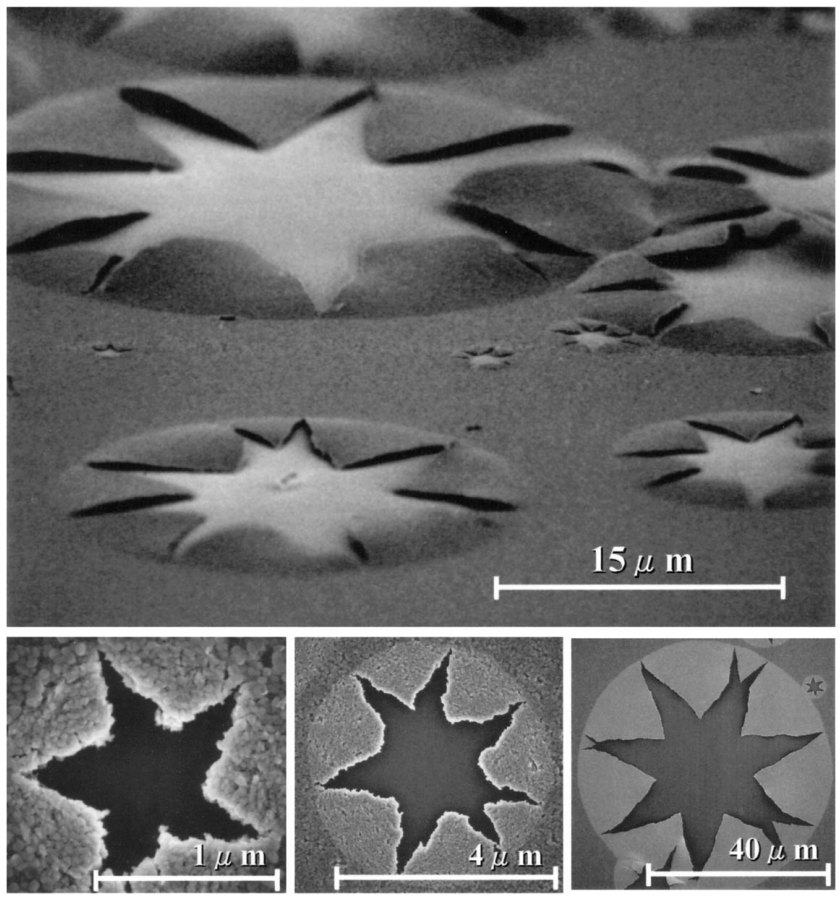

Figure 4 SEM micrographs of star-shape cracks with several sizes. All stars inscribe a real circle.

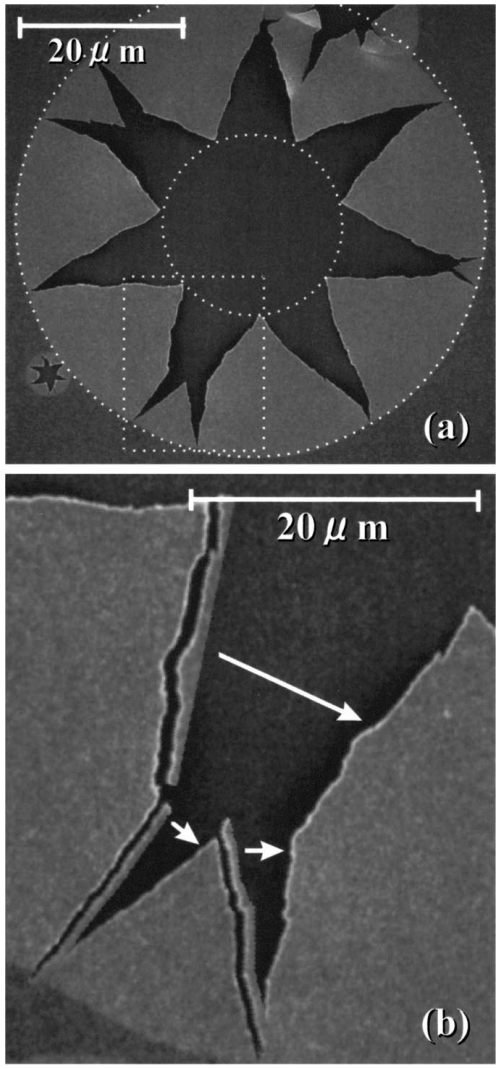

Figure 5 A star-shape crack which explains the reduction mechanism. In (a), the circles drawn inside and outside of the crack are concentric. In the enlarged photograph, (b), a facing edge of the crack is duplicated mechanically and put along the opposite edge. Facing edges were adjacent to each other before cracking.

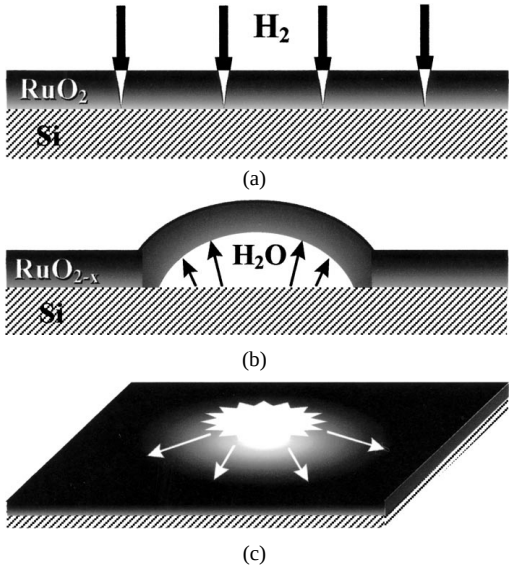

Figure 6 Precise process of the crack formation: (a) hydrogen gases diffuse through the RuO_2 film and reach to the RuO_2/Si interface; (b) the film is peeled off at the RuO_2/Si interface by forming a dome which maintains the pressure of the water vapor generated by the hydrogen reduction; (c) the reduction process across the film toward the surface, then the radical cracks are induced from its apex by the volume shrinkage.

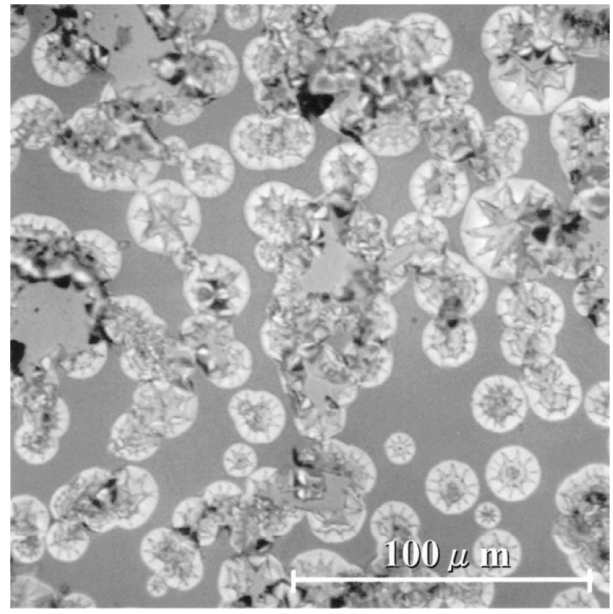

Figure 7 Optical microscope photograph of BST/RuO_2/Si structure after 0.3%-H_2 reduction at 200°C. The radical patterns are a little different those seen in RuO_2/Si.

The star-shape cracking due to the hydrogen reduction was still observed even when the RuO_2 film was covered with a 90-nm-thick BST film (Fig. 7). The radical patterns are a little different from those in Figs 3–5. This was plausibly because the mechanical strength of the dome holding the water vapor is enhanced by the BST cover. Fig. 8 shows x-ray diffraction patterns before (Fig. 8a) and after (Fig. 8b) hydrogen reduction of the BST/RuO_2 layered film. It is clear that the diffraction line intensity of RuO_2 (indexed with *hkl*) decreases, but the relative intensity of the line corresponding to Ru metal (indexed with *hkl**) increases after hydrogen reduction. On the other hand, the diffraction pattern of the BST film similar to that of the as-deposited

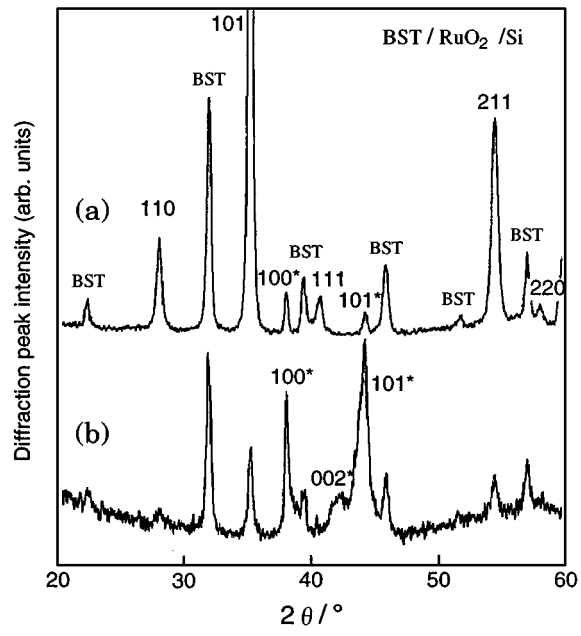

Figure 8 x-ray diffraction patterns of BST/RuO_2/Si structure: (a) as-deposited and (b) after 0.3%-H_2 reduction at 200°C. The BST is almost intact, while RuO_2 is reduced to Ru.

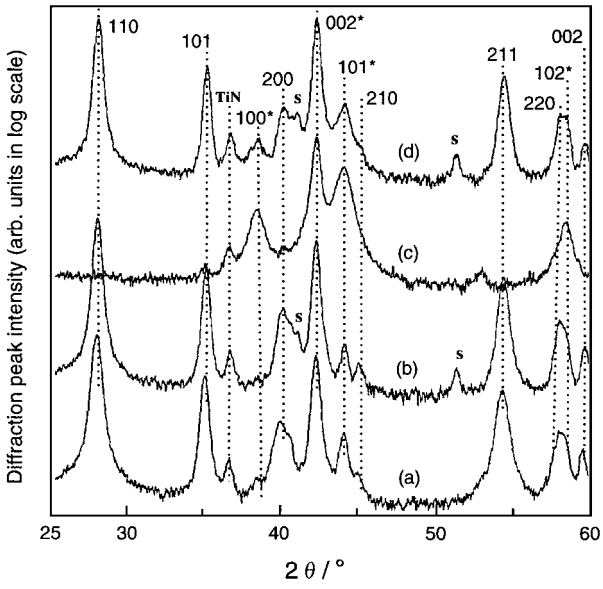

Figure 9 x-ray diffraction patterns of RuO_2/Ru/TiN/Ti/Si: (a) as-deposited, (b) after O_2-heat treatment at 700°C, (c) after 0.3%-H_2 reduction at 200°C and (d) after 0.3%-H_2 reduction at 200°C via O_2-heat treatment at 700°C. ("s" denotes the titanium silicide produced by the heat treatment.) Indices *hkl* and *hkl** indicate RuO_2 and Ru, respectively. The RuO_2 film is not apparently reduced in (d).

one was observed after the reduction, although the intensity decreased due to the increased surface roughness. These results indicate that the hydrogen gas diffused through the BST film, without decomposing it, and then reduced the RuO_2 film. This selective reduction is a result of the critical oxygen pressure for oxide decomposition of RuO_2 being much higher than that for BST [13].

3.2. Hydrogen reduction of RuO_2 film on a Ru/TiN/Ti/Si structure

The RuO_2 films formed on the Ru(50-nm thick)/TiN(80-nm thick)/Ti(50-nm thick)/Si substrate were reduced in 0.3% H_2/Ar atmosphere at 200°C. Fig. 9 shows the change in x-ray diffraction patterns after hydrogen reduction. Pattern (a) represents the as-deposited RuO_2/Ru/TiN/Ti/Si layered film. Pattern (b) represents the layered film once heat-treated in O_2 at 600°C. And patterns (c) and (d) represent the hydrogen-reduced films corresponding to patterns (a) and (b). The diffraction peaks marked with s are assigned to titanium silicide that was formed by heat-treatment at 600°C. The x-ray pattern of RuO_2 (indexed with *hkl*) almost unchanged after heat treatment in O_2 at 600°C [patterns (a) to (b)]. However, the heat treatment affected both of the x-ray pattern and the morphology after hydrogen reduction. When the as-deposited RuO_2 film was hydrogen-reduced, all diffraction lines of RuO_2 disappeared [pattern (c)], and the film was broken into pieces and peeled off along the whole RuO_2/Ru interface (Fig. 10a). The hydrogen gas can penetrate into the peeled-off interface in addition to the RuO_2 surface. As a result, it is thought that the RuO_2 film was completely reduced to Ru metal. It is difficult to investigate the change in the Ru diffraction peaks after hydrogen reduction because the lower structure also consists of a Ru metal layer. The increase of Ru peak height in Fig. 9, pattern (c) may therefore have resulted from the lower Ru being exposed.

On the other hand, when the RuO_2 film was reduced via heat treatment in O_2 (d in Fig. 9), the intensity of RuO_2 diffraction lines hardly changed. But the heat-treated RuO_2 film was also evidently reduced according to the film morphology in Fig. 10b. The RuO_2 film burst, leaving a crater from which the water vapor spouted out by the same mechanism as explained in Fig. 6. The RuO_2/Ru interface adhered next to craters, suggesting the post-heat treatment caused the interdiffusion and the strengthened adhesion.

Consequently, the RuO_2 film is reduced exclusively from the bottom interface, although the surface morphologies of the RuO_2 film on Si (Fig. 3) and that on

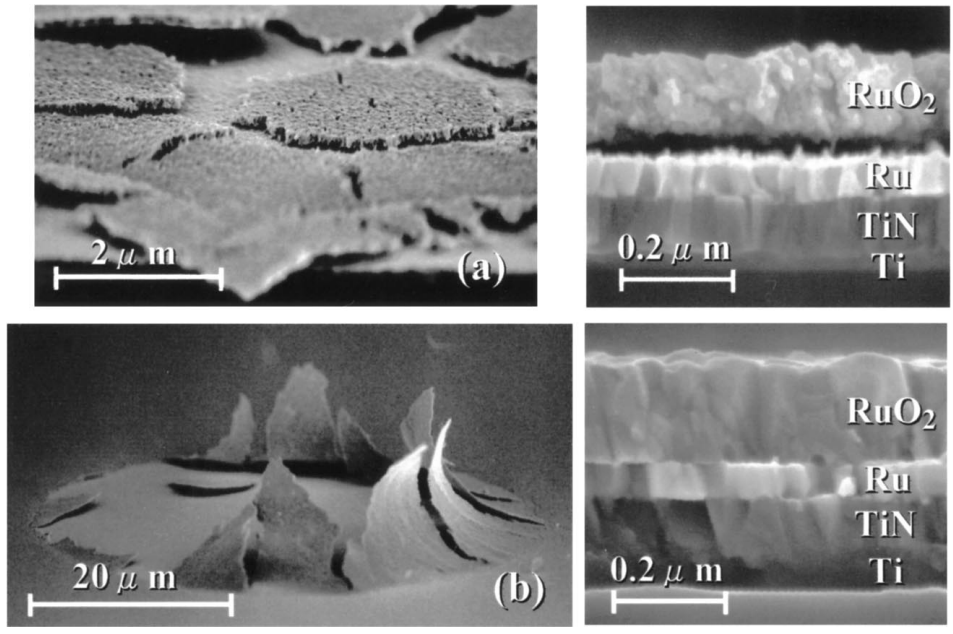

Figure 10 SEM micrographs of RuO_X/TiN/Ti/Si: (a) after 0.3%-H_2 reduction at 200°C [the same film as in Fig. 9c], (b) after 0.3%-H_2 reduction at 200°C via O_2-heat treatment at 700°C [the same film as in Fig. 9d]. The crater shows the RuO_2 was reduced and the water vapor spouted according to the same mechanism as shown in Figs 3 and 6.

Ru (Fig. 10) look different. The morphological destruction can not be prevented as long as the thermodynamic equilibrium is attained during the hydrogen reduction process.

4. Conclusions

Hydrogen reduction of a RuO_2 film prepared by reactive DC sputtering was investigated. The RuO_2 film is reduced to Ru metal selectively from the bottom interface after the hydrogen reduction in 0.3%-H_2/Ar at 200°C. Water vapor generation and volume shrinkage caused by the hydrogen reduction crack the RuO_2 films into a star shape. Similar cracking is still observed even when the RuO_2 film is covered with a 90-nm-thick BST film. The mechanical strength and the adhesion of RuO_2 can be improved to some extent by post-oxidation at high temperatures. However, no way to prevent the structural destruction can be found from the viewpoint of thermodynamic equilibrium. Therefore, the RuO_2 electrode cannot easily tolerate the hydrogen reduction process that is necessary for fabricating DRAMs.

References

1. M. L. GREEN, M. E. GROSS, L. E. PAPA, K. J. SCHNOES and D. BRASEN, *J. Electrochem. Soc.* **132** (1985) 2677.
2. Q. X. JIA, X. D. WU, S. R. FOLTYN, A. T. FINDIKOGLU, P. TIWARI, J. P. ZHENG and T. R. JOW, *Appl. Phys. Lett.* **67** (1995) 1677.
3. J. S. LEE, H. J. KWON, Y. W. JEONG, H. H. KIM and C. Y. KIM, *J. Mater. Res.* **11** (1996) 2681.
4. A. GRILL, W. KANE, J. VIGGIANO, M. BRADY and R. LAIBOWITZ, *ibid.* **7** (1992) 3260.
5. E. KOLAWA, F. C. T. SO, E. T.-S. PAN and M.-A. NICOLET, *Appl. Phys. Lett.* **50** (1987) 854.
6. L. K.-ELBAUM and M. WITTMER and D. S. YEE, *ibid.* **50** (1987) 1879.
7. S. SAITO and K. KURAMASU, *Jpn. J. Appl. Phys.* **31** (1992) 135.
8. K. TOKASHIKI, K. SATO, K. TAKEMURA, S. YAMAMICHI, P.-Y. LESAICHERRE, H. MIYAMOTO, E. IKAWA and Y. MIYASAKA, in Proc. 15th Symp. Dry Process, Tokyo, 1994 (Institute of Electrical Engineers of Japan, Tokyo, 1994) p. 73.
9. K. TAKEMURA, H. YAMAGUCHI, P.-Y. LESAICHERRE, K. TOKASHIKI, H. MIYAMOTO, H. ONO, Y. MIYASAKA and M. YOSHIDA, *Jpn. J. Appl. Phys.* **34** (1995) 5224.
10. Y. T. KIM and C. W. LEE, *ibid.* **35** (1996) 6153.
11. J.-H. AHN, W.-Y. CHOI, W.-J. LEE and H.-G. KIM, *ibid.* **37** (1998) 284.
12. W. F. MCCLUNE (ed.), "Powder Diffraction File" (JCPDS, Swarthmore, 1985).
13. J. A. RARD, *Chemical Reviews* **85** (1985) 1.

Received 2 July 1999
and accepted 16 February 2000